

Chapter 6

Prediction of Rare Earth $A_2Hf_2O_7$ Pyrochlore Phases

“If, without disturbing a system, we can predict with certainty the value of a physical quantity, then there exists an element of physical reality corresponding to this physical quantity.”

- Albert Einstein

Physical Review, 1935

6.1 Introduction

Materials with the pyrochlore lattice exhibit properties that are advantageous for applications as diverse as dielectrics [199,200] and actinide host phases [208,211]. However, the phase stability for any $A_2B_2O_7$ pyrochlore compound (where A is a 3+ rare earth cation ranging in size from Lu^{3+} to La^{3+} and B is a 4+ cation ranging in size from Ti^{4+} to Pb^{4+}) is not well characterized. Limited and at times conflicting phase diagrams exist for the series of compounds $A_2Zr_2O_7$ and $A_2Ti_2O_7$

(refer to Figures 5.1, 5.2 and 5.3 for titanates and Figures 5.5 and 5.6 for zirconates). However, there is a more complete set of data showing the existence of certain $A_2Hf_2O_7$ compounds (refer to Figures 5.9, 5.10 and 5.11).

Considering this latter series further, the $HfO_2 - Pr_2O_3$ and $HfO_2 - La_2O_3$ phase diagrams [238], both exhibit a considerable pyrochlore phase field which melts congruently (i.e. the liquid is the same composition as the compound) at 2420°C and $2460^\circ\text{C} \pm 25^\circ\text{C}$ respectively. The $HfO_2 - Nd_2O_3$ and $HfO_2 - Sm_2O_3$ phase diagrams [237, 238] similarly exhibit significant pyrochlore phase fields, but both melt incongruently at 2450°C and $2550^\circ\text{C} \pm 25^\circ\text{C}$ respectively. The $HfO_2 - Tb_2O_3$, $HfO_2 - Gd_2O_3$ and $HfO_2 - Eu_2O_3$ phase diagrams [237, 252] also exhibit a pyrochlore phase field, however, these do not melt but rather undergo an order-disorder transformation at 2150° , 2350°C and $2450^\circ\text{C} \pm 50^\circ\text{C}$ respectively. All $HfO_2 - A_2O_3$ phase diagrams with A smaller than Gd^{3+} , including $Dy_2O_3 - HfO_2$ [235, 237, 252, 253], show no evidence of pyrochlore compound formation. In all cases, the experimental error of the order-disorder temperature is given as denoted in the original texts.

Figure 6.1, although consisting of $A_2O_3 - HfO_2$ differs from those in Chapter 5. Each of the phase diagrams in Figure 6.1 was obtained from the original texts. Here, the transition from no pyrochlore phase observed for the $Dy_2O_3 - HfO_2$ system to a pronounced pyrochlore region in the $Tb_2O_3 - HfO_2$ is evident, as is the subsequent progression of the pyrochlore phase (i.e. the increase in order-disorder temperature) from $Gd_2O_3 - HfO_2$ up to $Eu_2O_3 - HfO_2$. The benefit of the original experimental data is that the temperatures at which the experiments are clearly labelled. This will be shown to be important in the forthcoming sections.

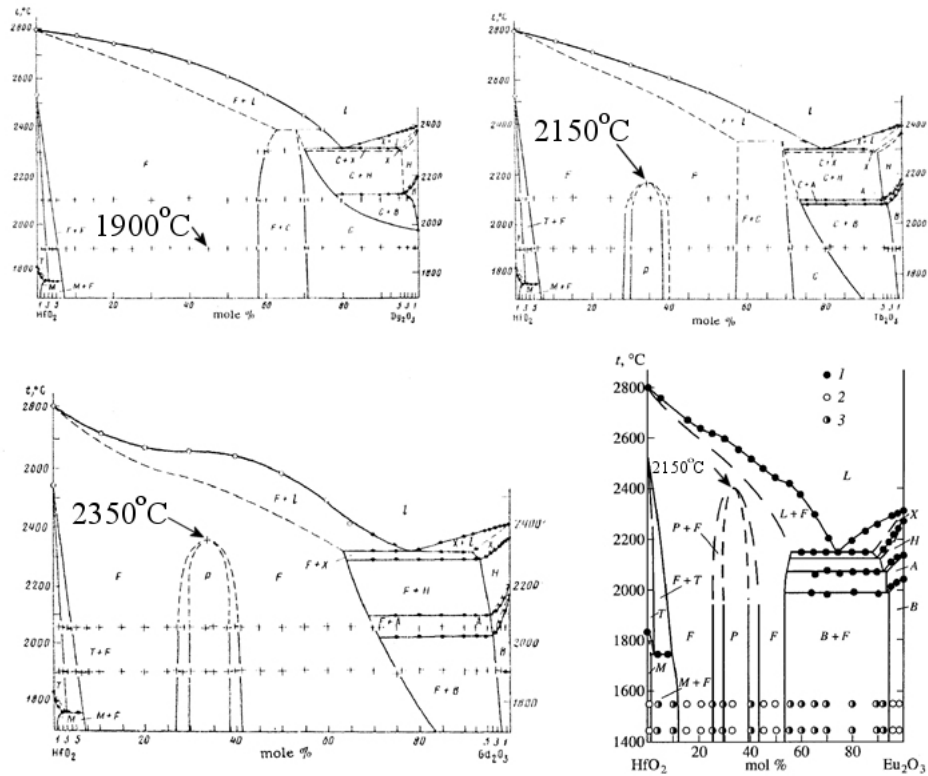


Figure 6.1: Phase diagrams of the $A_2Hf_2O_7$ series of compounds for intermediate A^{3+} , reproduced from [236, 237, 252].

The completeness of the $HfO_2 - A_2O_3$ series of phase diagrams allows us to compare this experimental data with atomistic simulation calculations. The simulations provide relative energies of a local disorder process for a wide range of pyrochlore compounds [243]. From these disorder energies and the aforementioned phase diagrams, it is possible to generate an Arrhenius-type plot of disorder temperature versus disorder energy, which predicts order-disorder temperatures for $Dy_2Hf_2O_7$ as well as $Ho_2Hf_2O_7$ and $Er_2Hf_2O_7$. These compounds have not been previously observed experimentally.

6.2 Methodology

Atomistic simulation calculations were carried out based on a Born like, ionic description of the lattice [79] and using the Buckingham potential to describe the short range interactions between ions (see Table 2.5 for the complete listing of potentials used). The polarizability of ions is accounted for by the shell model [109], where a massless shell of charge $Y|e|$ is coupled to a massive core of charge $X|e|$ by a force constant, k . All calculations consider O^{2-} and larger B^{4+} cations as polarisable. The shell parameters used can be found in Table 2.5. A comprehensive description of the Mott-Littleton defect calculation methodology is provided in Chapter 2 and elsewhere [254]. In all cases, calculations were carried out using the CASCADE code [127], which employs energy minimization to predict relaxed ion positions. The reader is referred to Chapter 2 for computational details.

The approach described has been used successfully to predict various properties of $A_2Hf_2O_7$ pyrochlores, including oxygen migration [244], disorder process energies [243] and the effect of disorder on the oxygen positional parameter [245].

6.3 Results and Discussion

By far the two most important disorder processes for pyrochlores are: cation antisite and anion Frenkel [250]. Cation antisite is essentially the swapping of an A^{3+} cation for a B^{4+} cation:

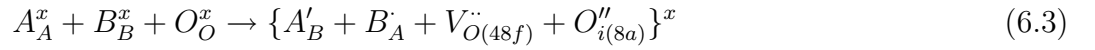


Frenkel anion disorder proceeds when an oxygen ion on a 48f site is displaced to an 8a interstitial site, thus leaving the 48f site unoccupied:



Previous simulation results [243] for both of these processes for an extensive range of pyrochlore compounds were presented in the form of contour maps. These clearly demonstrate the same trend for both cation antisite and anion Frenkel. That is, the enthalpy increases considerably with increasing B cation radius, while the increase in enthalpy with increasing A radius is less pronounced. These results are qualitatively supported by experimental studies [204, 255].

However, for the three series of pyrochlore compounds: $A_2Sn_2O_7$, $A_2Hf_2O_7$ and $A_2Zr_2O_7$, the extent of disorder at temperatures above 1000K is sufficient for defect clusters to form [245]. Therefore, the appropriate disorder reaction (as discussed in [243]) involves the formation of neutral defect clusters consisting of a cation antisite pair adjacent to an anion Frenkel pair:



The rationale for defect cluster formation in these systems has been established in previous publications [239, 242].

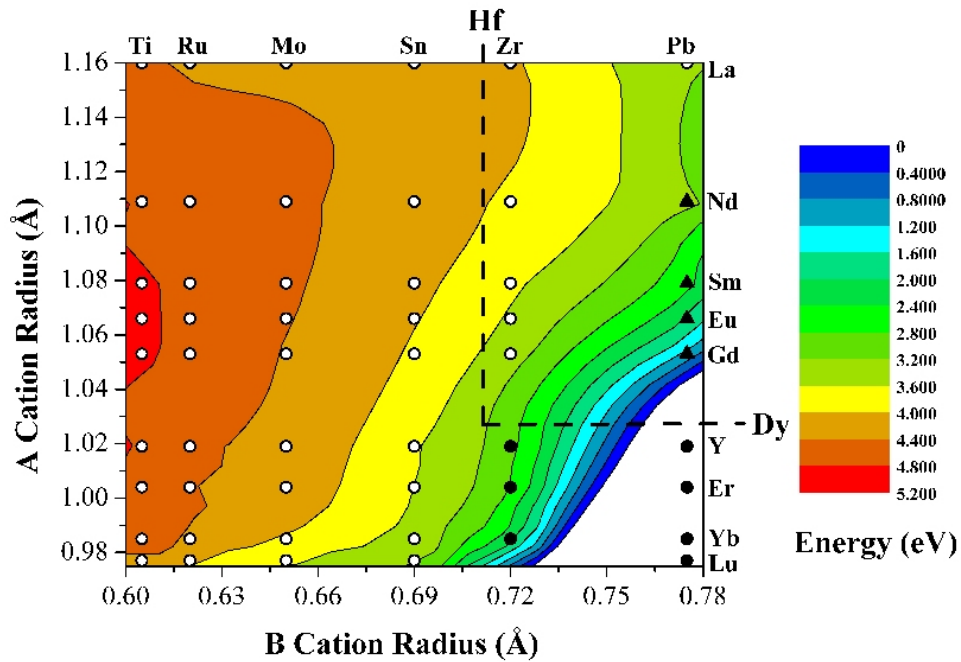


Figure 6.2: Contour map showing formation energies for combined cation antisite - anion Frenkel local disorder, highlighting the location of the compound $Dy_2Hf_2O_7$. Each composition for which a calculation was carried out is represented by a symbol whose meaning is discussed in the text.

Figure 6.2 is a contour map which displays the formation energies of this cluster for 54 pyrochlore compositions. Each point on the map refers to a specific composition for which a calculation was carried out. Open circles are stable pyrochlore formers, whereas filled circles have not been observed experimentally to form a pyrochlore structure. The filled triangle symbols are compositions that have been observed once to form pyrochlores but only when synthesized under high pressure (300MPa) [256]. Further information on these contour maps can be found in Section 5.2.1.

A useful characteristic of contour maps is their ability to predict properties of compounds for which calculations were not explicitly carried out. For example, al-

though calculations have not been performed for $Dy_2Hf_2O_7$, the disorder energy can be extracted from the contour map, as shown in Figure 6.2 (Dy ionic radius = 1.027\AA and Hf ionic radius = 0.71\AA [6]). Indeed, disorder energies can be obtained from this map for the entire series of $A_2Hf_2O_7$ pyrochlores, despite not calculating the values explicitly.

If the local disorder energy for each $A_2Hf_2O_7$ pyrochlore obtained from Figure 6.2 is correlated with the known disorder temperature (via an Arrhenius plot [257], see Figure 6.3), it is found that there is, within experimental error, a linear relationship. Such an observation supports the idea that, for each compound of this series, the local disorder energy is related to an order - disorder enthalpy. Of course, our local order - disorder internal energies are incomplete compared to order - disorder free energies. Consequently, further work is being carried out in order to develop a more thorough thermodynamic interpretation.

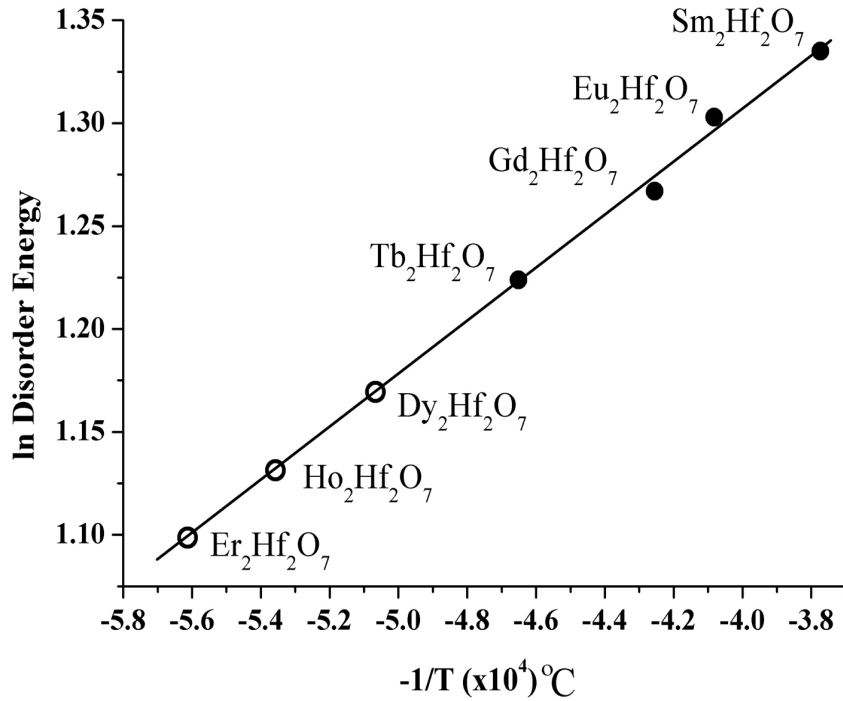


Figure 6.3: An Arrhenius plot of local disorder energy versus temperature. From the linear fit of the pyrochlore formers (solid points), it is possible to predict formation temperatures for three other compounds: $\text{Dy}_2\text{Hf}_2\text{O}_7$, $\text{Ho}_2\text{Hf}_2\text{O}_7$ and $\text{Er}_2\text{Hf}_2\text{O}_7$.

Despite its approximate nature, there exists a useful relationship which, via Figure 6.3, can be used to predict order - disorder temperatures for compositions which have not yet been observed in the pyrochlore structure, but only as fluorite solid solutions. For example, it is clear from Figure 6.3 that, next to those pyrochlores already observed, $\text{Dy}_2\text{Hf}_2\text{O}_7$ will be the composition with the highest predicted order - disorder temperature: $1975^\circ\text{C} \pm 50^\circ\text{C}$.

It is now possible to revisit the region of the $\text{Dy}_2\text{O}_3 - \text{HfO}_2$ phase diagram where a $\text{Dy}_2\text{Hf}_2\text{O}_7$ pyrochlore should be observed, see Figure 6.1. The experimental points from which the phase diagram was constructed ($1900^\circ\text{C} \pm 50^\circ\text{C}$) are found to be at

the threshold temperature of a stable pyrochlore, as indicated by points in Figure 6.1. Conversely, order - disorder temperatures predicted for $Ho_2Hf_2O_7$, $1865^\circ C \pm 50^\circ C$ and $Er_2Hf_2O_7$, $1780^\circ C \pm 50^\circ C$ are well below the experimental data points.

The aim of this prediction is to stimulate experimental investigation. The recent work of Helean *et al.* [258] lends itself to verifying the prediction of this chapter. Using high temperature oxide melt calorimetry, Helean *et al.* have derived enthalpies of formation for several pyrochlores.